Magneto-optical properties of CrO_2

H. Brändle,* D. Weller, S. S. P. Parkin, and J. C. Scott
IBM Research Division, Almaden Research Center, San Jose, California 95120

P. Fumagalli, W. Reim,† R. J. Gambino, and R. Ruf
IBM Research Division, Thomas J. Watson Research Center, Yorktown Heights, New York 10598

G. Güntherodt
II. Physikalisches Institut, Rheinisch-Westfälische Technische Hochschule Aachen, W-5100 Aachen, Germany
(Received 20 April 1992)

The magneto-optical, polar Kerr effect of polycrystalline CrO_2 has been studied in the range 0.8–5 eV. The maximum Kerr rotation amounts to $|\theta_K| = 0.154°$ at 3.7 eV. Two different interpretations of the observed magneto-optical transitions are discussed: (1) based on published spin-polarized band-structure calculations and (2) based on published spin-polarized photoemission data. Additional transport measurements are made to elucidate the free-electron contributions. At room temperature, the electrical resistivity is 190 $\mu\Omega$ cm, while Hall measurements show a carrier concentration of 0.5 e/f.u. in a one-band model. Because of a small Kerr effect of $|\theta_K| < 0.1°$ in the energy range 1.5–3 eV and a low reflectivity of less than 30%, CrO_2 is not attractive for magneto-optical recording.

I. INTRODUCTION

Despite its widespread use as particulate magnetic recording medium in tapes, little attention has been paid so far to the magneto-optical properties of CrO_2, which is surprising, as it might also be suitable for magneto-optical recording. CrO_2 crystallizes in the tetragonal rutile structure and orders ferromagnetically well above room temperature with a Curie temperature of $T_C = 391$ K.[1] Two features make it a possible candidate for a material with a large Kerr effect at room temperature: (1) a pronounced plasma edge near 1.2 eV in optical reflectivity spectra of CrO_2 reported by Chase[2] and (2) the prediction of half-metallic ferromagnetism in CrO_2, i.e., metallic character of majority and semiconducting character with a band gap for minority spins, by Schwarz in 1985.[3] These phenomena can lead to large magneto-optical effects as demonstrated, e.g., in PtMnSb (Ref. 4) and $CuCr_2Se_4$,[5] both of which show Kerr rotation angles $|\theta_K| > 1°$ at room temperature. In the case of CrO_2, an indication of the plasma edge enhancement might have been observed in Kerr effect measurements by Stoffel in 1969.[6] The onset of a resonance-type feature near 1.2-eV photon energy, which marked the lower energy limit in this early report, however, could not be interpreted unequivocally. Here we report a comprehensive study of the magneto-optical properties of CrO_2 in the 0.8–5 eV range, using the magneto-optical Kerr effect as well as Faraday rotation measurements. We show that our optical and magneto-optical data can be interpreted within the framework of spin-polarized band-structure calculations.[3]

We also compare our results with recent spin-polarized photoemission results, which revealed a 90% spin polarization at 2-eV binding energy but vanishing density of states near the Fermi level.[7] Our resistivity and Hall measurements as well as the optical data are distinctly different from the photoemission (PES) results as they unambiguously show a considerable free-carrier concentration at the Fermi energy. A possible explanation for this discrepancy will be discussed.

II. SAMPLE PREPARATION AND CHARACTERIZATION

For our Kerr effect, optical and transport measurements, a 1.3-μm-thick CrO_2 film was used. It was obtained by chemical vapor deposition by decomposing CrO_3 at 200 °C in a closed reactor onto (0001) cut sapphire. The substrate temperature was 390 °C. X-ray diffraction showed exclusively (200) and (400) peaks with d spacings in accordance with literature data,[8] indicating highly textured growth with the a axis normal to the film surface. The second a axis and the c axis were isotropically distributed in the film plane, as will be discussed later. The room-temperature magnetization was determined most accurately from the saturation field of a hard axis polar Kerr loop to be $M_s = 475 \pm 5$ emu/c.c., in agreement with the data of $M_s = 480$–528 emu/c.c. reported by Chamberland.[1] The temperature dependence of the magnetization, shown in Fig. 1, was measured with a SQUID magnetometer. The film thickness was evaluated by normalizing the measured total moment at 0 K to the reported moment of $2.00 \pm 0.05 \mu_B$ per CrO_2 (Ref. 1), and determined to be 1320 nm. Using this thickness we find $M_s = 471$ emu/c.c. at 297 K from the SQUID measurement and $M_s = 477$ emu/c.c. from an independent vibrating sample magnetometry measurement.

Because Faraday effect measurements require an isotropic and transparent substrate, the respective films were grown onto fused quartz, which was additionally seeded with a polycrystalline TiO_2 buffer layer to estab-

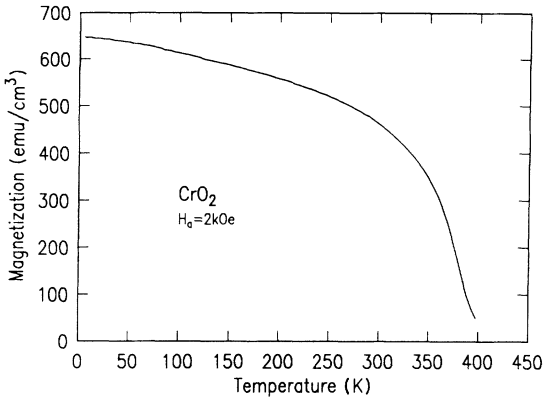

FIG. 1. Temperature-dependent magnetization of CrO_2 measured with a SQUID magnetometer.

lish polycrystalline growth of CrO_2. X-ray diffraction showed a $\langle 110 \rangle$ texture, i.e., a slightly different preferential orientation compared to the film used for the Kerr effect, the optical, and the transport measurements.

III. OPTICAL PROPERTIES

The normal incidence reflectivity R was calculated from optical constants n and k, as measured by ellipsometry in the range 1.4–3.5 eV with a Gaertner spectroscopic ellipsometer via

$$R=\frac{(n-1)^2+k^2}{(n+1)^2+k^2} . \tag{1}$$

The accuracy in the measured optical constants n and k was ± 0.01. The infrared (IR) and ultraviolet (uv) reflectivity was accessed by relative measurements using a Perkin Elmer Lambda 9 spectrometer. As reference mirrors, we used a freshly evaporated Au film for the range 0.4–2 eV and a MgF_2 coated Al mirror (Oriel) for the range 2.5–5 eV. R was then obtained by scaling to the ellipsometrically determined, absolute reflectivity between 1.4 and 3.5 eV, assuming constant R of the reference mirrors in the respective energy ranges. Scaling factors of 0.975 and 0.925 for Au and Al, respectively, are consistent with published data.[9] Starting from the measured optical constants in the range 1.4–3.5 eV, n and k were recursively extrapolated into the IR and uv using the boundary condition that n and k are consistent with the normal-incidence reflectivity according to Eq. (1).

Figure 2 shows the normal-incidence reflectivity between 0.4 and 5 eV at room temperature. The present reflectivity data are in quantitative agreement with Ref. 2. The steep reflectivity drop from 60 to 20 % in the infrared region is clearly associated with a plasma edge below 1.2 eV, as mentioned in the Introduction. The influence of the optical constants n and k near the plasma edge on the Kerr effect, often referred to as the optical constants effect, is shown in the inset of Fig. 1. Depicted are the prefactors

$$\frac{1}{\hbar\omega}\left[\frac{B}{A^2+B^2}\right]$$

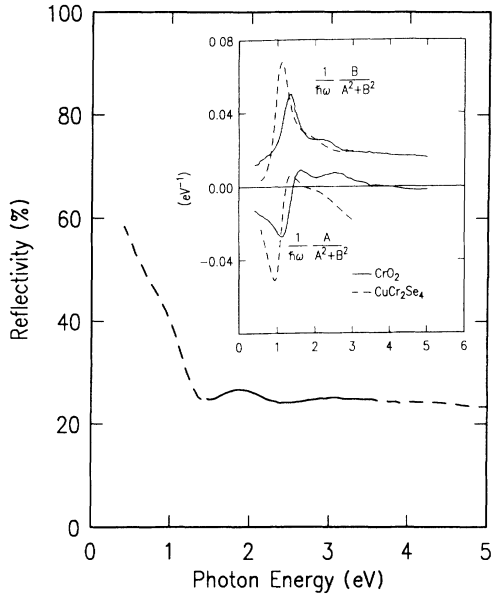

FIG. 2. Normal-incidence reflectivity R of CrO_2 at room temperature between 0.4 and 5 eV. The bold line indicates the reflectivity calculated from ellipsometrically determined n and k. The dashed lines indicate regions where a relative measurement was used to determine the reflectivity (see text). The inset shows functions of the optical constants n and k which enter Eqs. (2) and (3) for the magneto-optical Kerr effect as prefactors. The dashed lines are the corresponding prefactors for $CuCr_2Se_4$ (Ref. 5).

and

$$\frac{1}{\hbar\omega}\left[\frac{A}{A^2+B^2}\right],$$

which enter the polar Kerr rotation θ_K and Kerr ellipticity ε_K via the relations

$$\theta_K=\frac{4\pi}{\omega}\left[\frac{B}{A^2+B^2}\sigma_{1xy}+\frac{A}{A^2+B^2}\sigma_{2xy}\right] \tag{2}$$

and

$$\varepsilon_K=\frac{4\pi}{\omega}\left[\frac{A}{A^2+B^2}\sigma_{1xy}-\frac{B}{A^2+B^2}\sigma_{2xy}\right] . \tag{3}$$

$A=(n^3-3nk^2-n)$ and $B=(-k^3+3n^2k-k)$ are functions of the optical constants n and k and $\tilde{\sigma}_{xy}=\sigma_{1xy}+i\sigma_{2xy}$ denotes the off-diagonal element of the conductivity tensor $\tilde{\sigma}$. The resonancelike prefactors show a striking similarity to those obtained in $CuCr_2Se_4$ (Ref. 5), which are also shown in the inset of Fig. 2 (dashed curves). They are typical for metals with a pronounced plasma edge and their magnitude strongly depends on the separation in energy of free-carrier contributions and the onset of interband transitions.[10]

IV. MAGNETO-OPTICAL PROPERTIES

Room-temperature polar Kerr rotation and ellipticity spectra were measured in the range 0.8–5 eV, using a ful-

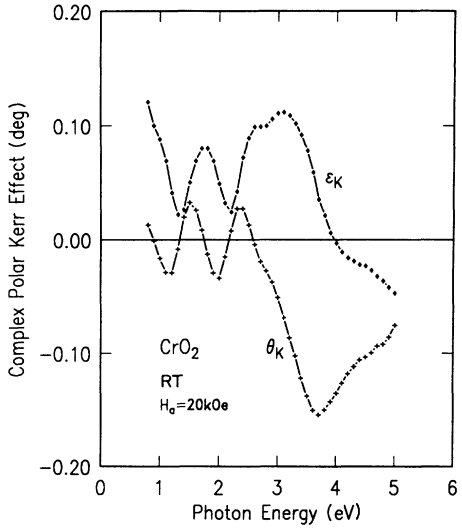

FIG. 3. Magneto-optical, polar Kerr rotation θ_K and the Kerr ellipticity ε_K of CrO_2 in the range 0.8–5 eV, measured at room temperature in an external, saturating magnetic field $H_a = \pm 20$ kOe.

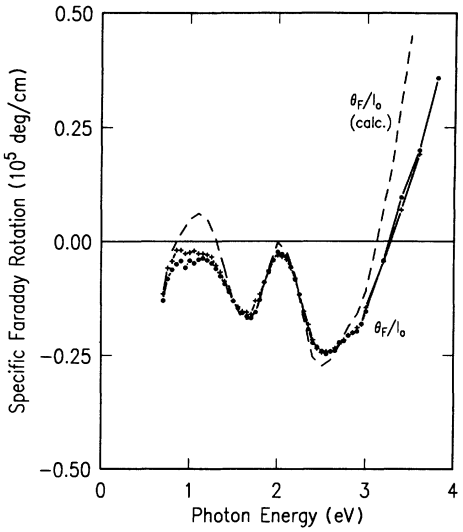

FIG. 4. The specific Faraday rotation between 0.7 and 3.8 eV. The directly measured Faraday rotation is indicated by symbols, while the dashed line shows the calculated specific Faraday rotation on the basis of measured θ_K, ε_K, n, and k.

ly automated spectrometer, based on a zeroing technique.[11] Magnetic fields up to ±20 kOe were applied to ensure magnetic saturation of the films. Reference measurement of a Pt mirror was used to correct for spurious contributions of Faraday rotation in optical elements, i.e., lenses, exposed to the stray field of the magnet. The relative error of the Kerr rotation is $<0.001°$ in the whole range, the absolute error is $<0.01°$ between 0.8 and 4.5 eV, increasing above 4.5 eV due to the influence of stray light. For the determination of the Kerr ellipticity, the principle of Senarmont was applied, using a tunable Soleil-Babinet phase shifter.[11] Kerr effect measurements for different orientations of the film plane relative to the polarization direction of the incident light beam did not show any changes, indicating isotropic distribution of a and c axes in the film plane.

Figure 3 shows the measured room temperature $\theta_K(\hbar\omega)$ and $\varepsilon_k(\hbar\omega)$ spectra in the energy range $0.8 \leq \hbar\omega \leq 5$ eV. The Kerr rotation shows a maximum value $|\theta_K| = 0.154°$ at 3.7 eV. It is significantly below 0.1° in the energy range between 1.5 and 3 eV (826–413 nm), which is the interesting region for applications in optical storage. The most significant result is the remarkably small Kerr rotation around 1.2 eV despite the presence of strong optical constant effects as demonstrated in the inset of Fig. 2. In order to confirm our results on the Kerr effect, the Faraday rotation θ_F was measured on two transparent samples between 0.6 and 3.8 eV at room temperature in an applied field of 10 kOe. To account for the substrate contribution a corresponding TiO_2/SiO_2 bilayer was measured as well. The film thicknesses were evaluated by measuring the absorption constant $K = 4\pi k/\lambda$ with λ the wavelength and k the ellipsometrically determined absorption index. These values, however, turned out to be about 20% larger than the values determined by Rutherford backscattering spectrometry (RBS).

Figure 4 shows the specific Faraday rotation between 0.7 and 3.8 eV for two different samples using the optically determined thicknesses. The dashed line corresponds to the calculated θ_F/l_0 according to Ref. 11:

$$\frac{\theta_F}{l_0} = -\frac{2\pi}{c}\left[\frac{n\sigma_{1xy} - k\sigma_{2xy}}{n^2+k^2}\right] \tag{4}$$

with l_0 the film thickness. σ_{1xy} and σ_{2xy}, which will be discussed below, were obtained via Eqs. (2) and (3) from the measured quantities θ_K, ε_K, n, and k. The agreement of the calculated and the measured specific Faraday rotation clearly confirms the present set of data on CrO_2. The deviation in the IR as well as in the uv is most likely due to different crystallographic orientations of the film used for the Kerr effect and the Faraday rotation measurement. A respective sensitivity of, e.g., optical constants on the crystallographic orientation in CrO_2, especially in the infrared, was reported earlier.[2]

V. TRANSPORT PROPERTIES

The electrical resistivity was measured using a low-frequency lock-in technique with a four in-line probe geometry. The present sample showed a specific resistivity of 190±20 $\mu\Omega$ cm at room temperature. A geometrical correction factor according to Ref. 12 was taken into account. Figure 5 shows the Hall resisitivity, measured at room temperature as a function of an applied magnetic field H_a up to 16 kOe. H_a was perpendicular to the film plane, i.e., parallel to the a axis of CrO_2. The sign of the Hall effect was calibrated with a silver and a copper film and the corresponding carrier concentrations were within ±10% of published data.[13] The overall error of the specific Hall resistivity is below ±30%. In order to determine the carrier concentration, the empirical ansatz

$$\rho_H = R_0 B + 4\pi R_s M \tag{5}$$

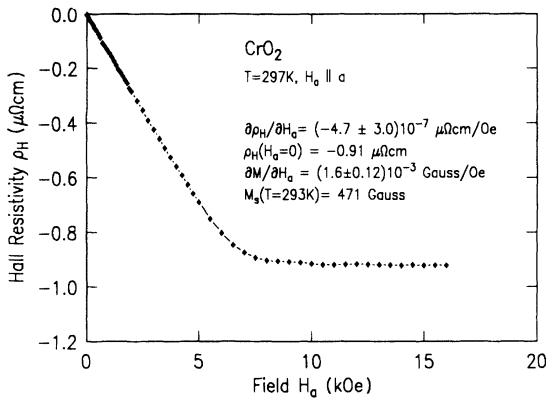

FIG. 5. Room-temperature Hall resistivity vs magnetic field in the range 0–16 kOe. The data for the calculation of the ordinary Hall coefficient R_0, according to Eq. (7), are indicated.

is used, with B the magnetic induction, M the magnetization, and R_0 and R_s the ordinary and extraordinary Hall coefficients, respectively. According to Ref. 13, R_0 can be derived using

$$R_0=\frac{\partial\rho_H}{\partial H_a}-\frac{\rho_H(0)}{M_s}\frac{\partial M}{\partial H_a} \tag{6}$$

with M_s the saturation magnetization. $4\pi R_s=\rho_H(0)/M_s$ is determined by linear extrapolation of ρ_H from high fields to $H_a=0$. The derivative $\partial M/\partial H_a$ was most accurately obtained by measuring the field dependence of the Kerr rotation which is proportional to the magnetization M. The advantage of the Kerr effect over conventional magnetic measurements for the measurement of $\partial M/\partial H_a$ in films is its insensitivity to spurious magnetic contaminations. The error in $\partial M/\partial H_a$ was below $\pm 8\%$. Due to the small slope, on the other hand, the error in $\partial\rho_H/\partial H_a$ was substantial. However, as the second term in Eq. (6) is dominating, the overall error in R_0 is estimated to be $<\pm 50\%$. In a one-band model, the carrier concentration N can finally be determined according to

$$R_0=-\frac{1}{Ne}\ , \tag{7}$$

where e is the electron charge. We find N in the range 0.32–0.96 electrons per formula unit (f.u.), with a mean value $\bar{N}=-1/\bar{R}_0 e=0.49$ e/f.u.

VI. INTERPRETATION

An interpretation of the Kerr spectra in terms of the interband transitions involved by analysis of the conductivity tensor $\tilde{\sigma}$ is carried out in Figs. 6(a) and 7. The off-diagonal elements $\tilde{\sigma}_{xy}=\sigma_{1xy}+i\sigma_{2xy}$ have been evaluated from the measured Kerr spectra and optical constants according to Eqs. (2) and (3). Symbols in Fig. 6(a) represent directly measured data points, lines are based on derived n and k values as discussed above. The value of σ_{1xy} at $\omega=0$ was calculated from the transport properties according to Ref. 11 with

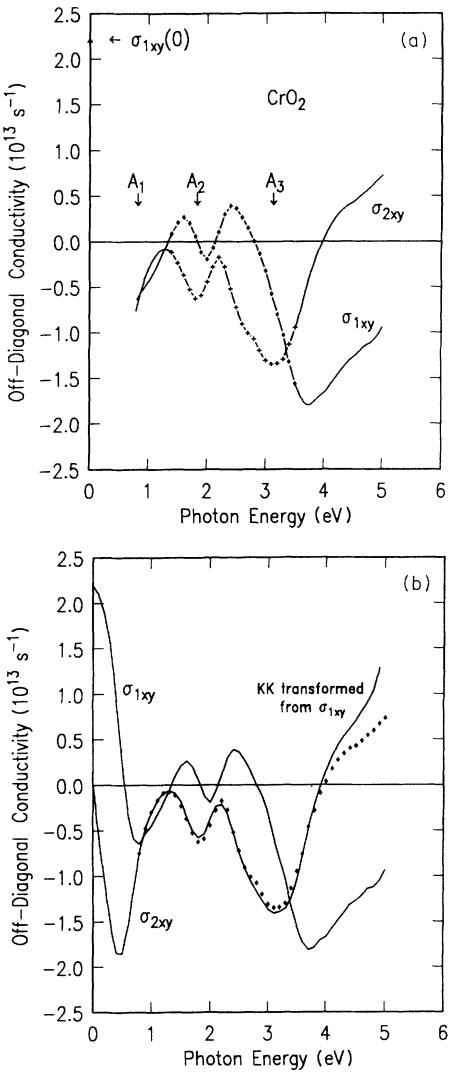

FIG. 6. (a) Complex off-diagonal conducivity spectra. The bold lines indicate regions where approximated values for n and k were used (see text). The labels A_1-A_3 indicate interband transitions discussed in the text. The value $\sigma_{1xy}(0)$, as derived from the transport measurements, is also indicated. (b) The line for σ_{2xy} shows the calculated spectrum by transforming σ_{1xy} with the Kramers-Kronig relation. The symbols are the independently determined values, shown in (a). The extrapolation of σ_{1xy} to the value at $\omega=0$, derived from transport measurements, was optimized to give the best correspondence with the independently determined values σ_{2xy}.

$$\sigma_{1xy}(\omega=0)=-\frac{\rho_H}{\rho^2}\ . \tag{8}$$

Herein, ρ and ρ_H are the specific resistivity and Hall resistivity, respectively. A good test for the consistency of the present data set is the extrapolation to the low-energy side of $\sigma_{1xy}(\omega)$ and subsequent calculation of σ_{2xy}, using the Kramers-Kronig (KK) relations. The result is shown in Fig. 6(b), with the symbols representing the values given in Fig. 6(a). The deviation between the experimental and the KK transformed $\sigma_{2xy}(\omega)$ at the

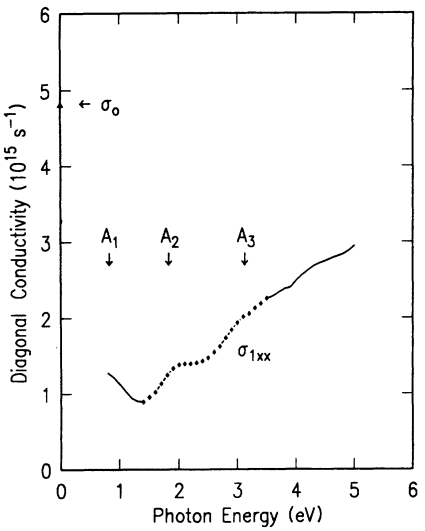

FIG. 7. The absorptive part σ_{1xx} of the diagonal element of the conductivity tensor. σ_0 is the conductivity derived from resistivity measurements (see text).

high-energy end of the spectrum is mainly due to the cutoff in $\sigma_{1xy}(\omega)$ at 5 eV. The agreement below 3.8 eV is excellent.

To support the interpretation of the present $\tilde{\sigma}_{xy}$ spectra, we also show in Fig. 7 the corresponding σ_{1xx} spectrum, as determined from the optical constants via

$$\sigma_{1xx}=\frac{\omega}{4\pi}\varepsilon_2=\frac{\omega}{4\pi}2nk\ . \tag{9}$$

Both diagonal and off-diagonal conductivity elements define the line shape and therefore the electronic nature of a magneto-optical transition. A feature in σ_{2xy} can either be absorptive or dispersive, for historical reasons referred to as paramagnetic or diamagnetic, respectively. The correlation with a feature in σ_{1xx}, which is always absorptive, makes it possible to determine the transition energy and therefore to distinguish the two types of magneto-optical transitions.

The well-structured spectral dependence of the off-diagonal conductivity arises from the superposition of several magneto-optically active transitions. Though not completely unequivocal, we show a consistent assignment of the features in Figs. 6(a) and 7 to electronic transitions A_1-A_3. The most obvious transition, that we have labeled A_2, is reflected in a distinct feature in σ_{1xx} near 2-eV transition energy. The corresponding feature in σ_{2xy} has a paramagnetic line shape and a transition energy of 1.8 eV. The other obvious feature, although only faint in σ_{1xx}, appears in σ_{2xy} at $\simeq 3.1$ eV. It is labeled A_3 and also has a paramagnetic line shape. A third transition A_1 is assigned to 0.8-eV photon energy, which marks the low-energy limit of the spectral range. It is indicated in σ_{1xx} as a feature superimposed to the free-electron contribution to σ_{1xx}. Moreover, it is clearly visible as a minimum in σ_{1xy} in Figs. 6(a) and 6(b), respectively. A possible structure above 4 eV is not discussed due to experimental uncertainties in n and k in that range.

The spectral dependence of $\tilde{\sigma}_{xy}$ shows similar features as reported by Dissanayake and Chase in $\Delta\varepsilon_2$ in thermoreflectance studies of CrO_2 with $E\|c$.[14] Herein, ε_2 is the absorptive part of the dielectric constant, which is proportional to σ_{1xx}, as shown in Eq. (9). The correspondence of the spectral dependence of $\Delta\varepsilon$ to our results is striking and we have therefore adapted the nomenclature of the above authors.[14] They explain the transitions observed in their experiment on the basis of a qualitative energy-band model proposed by Goodenough.[15]

VII. DISCUSSION

Different models have been discussed to account for the electronic structure and the ferromagnetic ordering in CrO_2. A recent approach by Schwarz[3] was a self-consistent, spin-polarized band-structure calculation. A semiquantitative comparison of the band-structure data of Schwarz[3] with our optical and magneto-optical results can be carried out by analyzing the joint density of states ($\mathcal{D}_J$), which we define as

$$\mathcal{D}_J(\hbar\omega)=\int_{E=0}^{\infty}N_{\rm occ}(E)\times N_{\rm em}(E+\hbar\omega)\times|M_{\rm occ,em}(E)|^2dE \tag{10}$$

with $N_{\rm occ}(E)$ and $N_{\rm em}(E)$ referring to the occupied and empty density of states, respectively. $|M_{\rm occ,em}|^2$ is the transition probability of the considered transition from occupied into empty states. Because of lack of information it is set equal to 1. The relation between σ_{1xx} and the above defined $\mathcal{D}_J$ is then given by

$$\sigma_{1xx}\propto\frac{\mathcal{D}_J(\hbar\omega)}{\hbar\omega}\ . \tag{11}$$

$\mathcal{D}_J/\hbar\omega$ is shown in Fig. 8. It was determined from the element-specific spin-up and spin-down density of states $N\uparrow(E)$ and $N\downarrow(E)$, respectively, published in Ref. 3. The total spin-resolved density of states according to Ref. 3 is shown in the inset of Fig. 8. The individual contributions to the $\mathcal{D}_J/\hbar\omega$ for spin-conserving ($N\uparrow\rightarrow N\uparrow$ and $N\downarrow\rightarrow N\downarrow$) and spin-flip transitions ($N\uparrow\rightarrow N\downarrow$ and $N\downarrow\rightarrow N\uparrow$), respectively, are distinguished by short- and long-dashed lines. Transition A_1 at 0.8 eV can be correlated to the corresponding distinct peak in $\mathcal{D}_J(\hbar\omega)/\hbar\omega$ for spin-conserving transitions and can therefore be assigned to a $d\uparrow$-$d\uparrow$ transition within the majority d bands near the Fermi level. Transition A_2 around 1.8 eV corresponds to a spin-flip transition from the occupied $d\uparrow$ states just below the Fermi level into $d\downarrow$ states above the Fermi level. The transition energy represents the exchange splitting, according to the band-structure calculations. Transition A_3 dominates in Fig. 6(a) and is much broader than A_1 and A_2. It is assigned to a $p(\mathrm{O})\rightarrow d(\mathrm{Cr})$ transition, although the band-structure calculation predicts these transitions above 3 eV, as shown in Fig. 8.

The assignment of the first two transitions on the basis of spin-polarized band-structure calculations explains the small Kerr effect in CrO_2 below 2.5 eV in a straightforward manner. In an atomic model, d-d transitions are

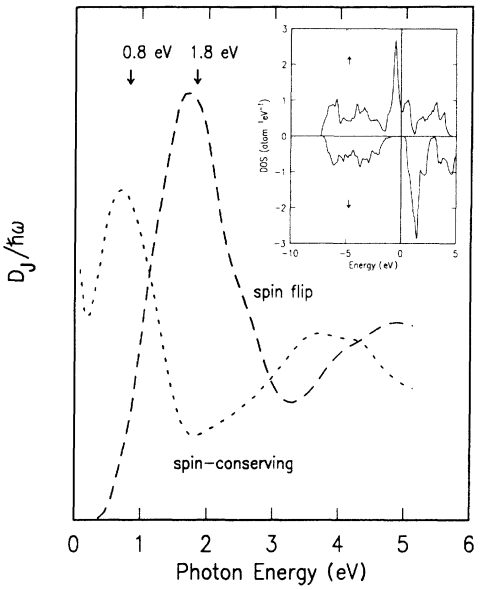

FIG. 8. $\mathcal{D}_J/\hbar\omega$ with $\mathcal{D}_J$ the joint density of states, computed on the basis of a spin-polarized band-structure calculation in Ref. 3. The short-dashed line corresponds to the spin-conserving, the long-dashed line to the spin-flip $\mathcal{D}_J$. The inset shows the spin-resolved density of states according to Ref. 3.

strictly dipole forbidden and become only partially allowed in solids, due to some admixture of, e.g., p character to the initial and final d states. This explains the small magneto-optical activity σ_{xy} near the A_1 transition in Fig. 6(a) and therefore the small Kerr rotation $|\theta_K| < 0.1°$ despite a pronounced optical constants effect near that energy. Spin-flip transitions, as A_2, are normally neglected because of their low transition probability compared to spin-conserving transitions. They become partially allowed through spin-orbit interaction, which is the responsible interaction for magneto-optical effects.

However, the correspondence of the peaks in $\mathcal{D}_J/\hbar\omega$ with the transitions A_1 and A_2 might be fortuitous. Usually, transition-metal oxides such as CrO_2 are assumed to have highly correlated d states, for which an appropriate description is the crystal-field theory rather than one-electron states used for the band-structure calculations. Indeed, recent photoemission experiments[7] are in disagreement with the spin-polarized band-structure calculations in Ref. 3 as the relevant density of states is found near 2-eV binding energy. Due to the nearly 100% spin polarization, it is assigned to $3d(\uparrow)$ states, whereas the band-structure calculation[3] predicts E_F to lie in the $3d(\uparrow)$ band. An alternative assignment of the optical transitions on the basis of the experimental spin-resolved photoemission data can be made if one assumes that the Fermi edge in that experiment is absent due to some oxygen deficiency at the surface, similar to the case of photoemission experiments from high-temperature superconductors.[16] This deficiency may also account for the weak emission intensity from s,p-derived states for binding energies between E_F and about 1 eV. Under these assumptions peak A_1 could then be attributed to a transition from s,p states below E_F into empty $d(\downarrow)$ states above E_F. A_2 may correspond to a transition from the $d(\uparrow)$ states near 2 eV below E_F into empty $d(\downarrow)$ states above E_F. The transition energy may be modified, i.e., reduced due to excitonic effects to yield the experimentally observed 1.8-eV transition energy. The A_3 peak can be accounted for by a transition from the occupied oxygen-derived p states near 3 eV below E_F into empty $d(\downarrow)$ states above E_F. Hence, under the above assumption of nonvanishing density of states at E_F, an assignment of the optical transitions can be made on purely experimental grounds. We outline this consistency because our Kerr effect, optical and transport measurements were carried out on samples of the same batch as the one used in the photoemission experiment.[7]

Also, we note that earlier photoemission experiments on powdered CrO_2 with Al K_α radiation [x-ray photoemission spectroscopy (XPS)], which is less surface sensitive, indicate a nonvanishing density of states at E_F.[17] Certainly, the absence of density of states near E_F in the photoemission experiment is not characteristic for bulk CrO_2 because the transport and the optical experiments as well as specific-heat measurements,[18] all of which are sensitive to the bulk properties, show metallic conductivity. Specific-heat measurements—carried out on samples of the same batch as used for the present study—reveal $\gamma = 7\ \mathrm{mJ\,K^{-2}\,mol^{-1}}$ in CrO_2, i.e., a considerable contribution of conduction electrons.[18] The electrical resistivity of 190 $\mu\Omega$ cm at room temperature is an order of magnitude higher than in Fe or Co but comparable to, e.g., Mn.[19] The residual resistivity at 0 K is about 1 $\mu\Omega$ cm.[20] The Hall measurements reveal an electron concentration of $\simeq 0.5$ e/f.u., assuming a one-band model. The free-electron contribution to σ_{1xx} was fitted by Chase with a Drude ansatz.[2] He found a plasma energy $\hbar\omega_p \simeq 2.0$ eV with a damping of $\hbar\gamma \simeq 0.15$ eV. Hence, we have to conclude that CrO_2 is a metal or at least a half-metal, in agreement with the conclusion drawn in a recent systematic study of transition-metal oxides.[21]

The nature of the states at E_F, however, is still unclear. Spin-polarized band-structure calculations indicate Cr $3d(\uparrow)$ at E_F.[3,22,23] On the other hand, the reported integer number of the magnetic moment of $2.00\mu_B$/f.u. (Ref. 1) indicates a filled d subband which does not cut the Fermi energy and therefore supports the photoemission results, as the observed $3d(\uparrow)$ band is well below E_F. In this case, the ferromagnetic coupling can be understood as a Ruderman-Kittel-Kasuya-Yoshida (RKKY) type interaction via the s,p states at the Fermi level, according to the interpretation by Goodenough.[15]

VIII. CONCLUSION

In summary, CrO_2 shows a small Kerr effect in the energy range of interest for applications despite considerable optical constants effect associated with a plasma edge in the reflectivity and in spite of the predicted half-metallic ferromagnetism. This is related to small transition probabilities of the involved transitions. Our results are consistent with reported bulk properties of CrO_2 and indicate metallic behavior of CrO_2.[1,2,14,18,20] Assuming

that the Fermi edge in a recent photoemission experiment is absent due to oxygen deficiency of the sample surface as was observed in high-temperature superconductors, our results can be interpreted on the basis of the spin-polarized photoemission studies. A different interpretation, based on a recent spin-polarized band-structure calculation, is also possible. However, it remains to be shown to what extent band-structure calculations can account for correlation effects in transition-metal oxides such as CrO_2.

The example of CrO_2 shows that a large Kerr effect due to optical constants effects can only be expected in conjunction with appropriate values in $|\sigma_{xy}|$. Moreover, if CrO_2 really belongs to the group of half-metallic ferromagnets, it is one more example—similar to the case of NiMnSb (Ref. 14)—that half-metallic ferromagnetism does not necessarily lead to large Kerr effects.

ACKNOWLEDGMENTS

We gratefully acknowledge G. L. Gorman, D. A. Hyde, and R. S. Swope for the x-ray analysis. We also thank N. Schubert and E. Wassermann of the University of Duisburg, Germany, for allowing us to include their specific-heat measurements.

*Present address: Balzers AG, FL-9496 Balzers, Fürstentum Liechtenstein.

†Present address: Siemens Medical Division MED-SMK, W-8520 Erlangen, Germany.

[1]B. L. Chamberland, Critical Rev. Solid State Sci. **7**, 1 (1977).

[2]L. L. Chase, Phys. Rev. B **10**, 2226 (1974).

[3]K. Schwarz, J. Phys. F **16**, L211 (1986).

[4]R. A. de Groot, F. M. Mueller, P G. van Engen, and K. H. J. Buschow, J. Appl. Phys. **55**, 2151 (1984); P. G. van Engen, K. H. J. Buschow, R. Jongebreur, and M. Erman, Appl. Phys. Lett. **42**, 202 (1983).

[5]H, Brändle, J. Schoenes, P. Wachter, F. Hulliger, and W. Reim, Appl. Phys. Lett. **56**, 2602 (1990); H. Brändle, J. Schoenes, P. Wachter, F. Hulliger, and W. Reim, J. Magn. Magn. Mater. **93**, 207 (1991).

[6]A. M. Stoffel, J. Appl. Phys. **40**, 1238 (1969).

[7]K. P. Kämper, W. Schmitt, G. Güntherodt, R. J. Gambino, and R. Ruf, Phys. Rev. Lett. **59**, 2788 (1987).

[8]B. J. Thamer, R. M. Douglass, and E. Staritzky, J. Am. Chem. Soc. **79**, 547 (1957).

[9]J. H.Weaver, C. Krafka, D. W. Lynch, and E. E. Koch, *Physik Daten* (Fachinformations-Zentrum Energie, Physik, Mathematik GmbH, Karlsruhe, 1981).

[10]H. Brändle, ETH Dissertation, 1990.

[11]W. Reim and J. Schoenes, in *Ferromagnetic Materials,* edited by E. P. Wohlfarth and K. H. J. Buschow (North-Holland, Amsterdam, 1990), Vol. 5, p. 133.

[12]H. H.Wieder, in *Materials Science Monographs,* edited by L. Larid (Elsevier Scientific, Amsterdam, 1979), Vol. 2.

[13]C. M. Hurd, *The Hall Effect in Metals and Alloys* (Plenum, New York, 1972).

[14]M. A. K. L. Dissanayake and L. L. Chase, Phys. Rev. B **23**, 6254 (1981).

[15]J. B. Goodenough, in *Progress in Solid State Chemistry,* edited by H. Reiss (Pergamon, Oxford, 1971), Vol. 5, p. 145.

[16]A. J. Arko, R. S. List, Z. Fisk, S.-W. Cheong, J. D. Thompson, J. A. O'Rourke, C. G. Olson, A.-B. Yang, Tun-Wen Pi, J. E. Schriber, and N. D. Shinn, J. Magn. Magn. Mater. **75**, L1 (1988).

[17]I. Ikemoto, K. Ishii, S. Kinoshita, H. Kuroda, M. A. Alario Franco, and J. M. Thomas, J. Solid State Chem. **17**, 425 (1976).

[18]N. Schubert and E. F. Wassermann (private communication).

[19]G. T. Meaden, *Electrical Resistance of Metals* (Plenum, New York, 1965).

[20]B. L. Chamberland, Mater. Res. Bull. **2**, 827 (1967).

[21]J. B. Torrance, P. Lacorre, C. Asavaroengchai, and R. M. Metzger, Physica C **182**, 351 (1991).

[22]E. Kulatov and I. I. Mazin, J. Phys.: Condens. Matter **2**, 343 (1990).

[23]S. Matar, G. Demazeau, J. Sticht, V. Eyert, and J. Kübler, J. Phys. (Paris) **2**, 315 (1992).